Turkish Journal of Electrical Engineering and Computer Sciences

Volume 6 | Number 3 Article 5

1-1-1998

FDTD Evaluation of the SAR Distribution in a Human Head Near a Mobile Cellular Phone

SELÇUK PAKER

LEVENT SEVGİ

ELEKTRİK, VOL.6, NO.3, 1998, ©TÜBİTAK

FDTD Evaluation of the SAR Distribution in a Human Head Near a Mobile Cellular Phone

Selçuk Paker
İTU Electronics and Communication Engineering Department,
Maslak 80626, İstanbul-TURKEY
e-mail: spaker@ehb.itv.edu.tr
Levent Sevgi
TÜBİTAK - MRC, Marmara Research Center, Information Technologies Research Institute
Gebze-Kocaeli, TURKEY
e-mail: levent-sevgi@mam.gov.tr

Abstract

In this study, Finite-Difference Time-Domain (FDTD) method is used to calculate the Specific Absorbtion Rate (SAR; defined as the power absorbed by unit mass of the tissue) distribution in a human head near a hand-held cellular phone. A three dimensional FDTD algorithm is built in cartesian coordinates. A discrete human head model, derived from a Nuclear Magnetic Resonance (NMR) image by semi-automatic algorithm, is located within FDTD volume together with a discrete hand-held receiver model. FDTD simulations are carried out for both european GSM (operating at 900MHz) and DECT (operating at 1.8GHz) systems with a quarter-wavelength antenna, mounted on top of the hand-held cellular phone. A new and an effective way of calcuating input, radiated and absorbed power distributions is introduced where time-domain Poynting vector is traced over a closed virtual surface surrounding the discrete phone and head models. SAR distributions for various vertical and horizontal slices of the human head are calculated and are shown to agree with the available calculation and measurement results. The computational results are interpreted in terms of international safety guideliness for human health.

1. Introduction

In the past few years, very rapid development in mobile cellular communication has drawn attention to possible health risks of the electromagnetic energy (EM) emitted from the transmitters of hand-held phones. The interaction between a human head and a hand-held phone under various conditions should be quantitatively evaluated in order to establish the safety in cellular mobile communication systems [1]. These evaluated values should be within the safety limits given in ANSI/IEEE C95.1-1992 RF Safety Guideless [2]. Three different limits are defined for the current safety studies: 1) a whole body avarge SAR; 2) a local peak SAR; and 3) a Specific absorption(SA), which limits the power of short pulses. Within these three, 1) and 2) must be avaraged over a defined period of time. Due to the high non-uniformity of the SAR distribution induced by a cellular mobile phone within a human head, the peak SAR is the relevant parameter to asses the risk caused by these devices. According to [2], in uncontrolled environments, a peak SAR of 1.6W/kg, as avarged over any 1 g of tissue must not be exceeded. But, according to [3], the limit on the peak SAR is

fixed at 1W/kg, as averaged over any 100g of tissue. The hand-held cellular mobile phone is stated to be safe in [2] when a cellular mobile phone's radiated power is less that 0.7 W (at 900MHz) and when the distance to human head is greater than 2.5 cm. Beside public biological concerns in cellular mobile communication system, there is also a great demand to know the deterioration of the antenna performance because of the existance of human head. This is an important feedback for antenna designers to develop better structures. Analyzing possible range of variations of the induced field strengths in various tissues requires an extensive efford, since local field strengths strongly depend on various parameters. Among the others

- operational frequency and antenna power
- mutual positions of the between device and -head
- design of the device
- size and the shape of human head
- distribution of tissues within the head
- electrical properties of the tissues

can be listed as important parameters which strongly affect the SAR distribution. Since some of the listed parameters are different for various individuals and can even change with time, analytical formulations (even the approximate ones) in SAR distribution calculations are extremely difficult.

The SAR distributions in a human head exposed to EM fields from hand-held cellular phones have been estimated through experimental [4-6], and numerical calculations [7-12]. The models used in these studies are quite different where from simple to enhanced geometries and from a few to many different tissue types are taken into account with different electrical properties. Morover, quite different values have been used in some of these studies [9] parallel to more accurate measurements of human tissues [13]. For example, there are more than hundred percent differences in some of the tissue parameters in [9]. Within the limits of the used models, these studies have presented the dependence of both local and global SAR distributions in a human head to the distance of the mobile cellular phone, as well as to its position. Also, it has been shown in these studies that SAR distributions within human neck and body casued by EM radiation above 300MHz are almost negligible. It is, therefore, quite acceptable to use isolated head and hand-held culluler phone during SAR distribution calculations.

Recent progress in computer technology enables us to use FDTD method to numerically calculate the EM interactions of a inhomogeneous, realistic human head and mobile phone models. In FDTD, spatial and time derivatives in Maxwell's equations are replaced with their central difference approximations in specially organized unit cells [14]. FDTD has been described in several publications and in a couple of recent books [15, 16]. In the unit cell, made up by $\Delta x \times \Delta y \times \Delta z$, six components of electromagnetic fields are arranged to minimize the computational storage needs [14]. The entire computation domain is obtained by stacking these unit cells into a larger rectangular volume. FDTD is very easy to implement and to trace the wave phenomen a and can handle complex geometries with inhomogeneous materials, either conductors or lossy dielectrics. FDTD has been applied to a large amount of EM problems, including planar microstrip analysis [17, 18], scattering and inverse scattering problems [16], [19], antenna simulation together with near-to-far field transformations [1] [15], [20], etc. Its comparison with other powerful time-domain techniques has also been presented [21].

In this study, EM interaction of a human head and a mobile phone is investigated by using an FDTD algorithm. Since the input and radiated powers determine the degree of this interaction, a new and effective

way of power calculation is introduced. Both volume (tripple) and closed surface (double) integrations of related field components are performed during FDTD simulations to obtain these power values. Also, absorbed power in lossy tissues is calculated in a similar way by using conductivity of a tissue at each FDTD cell. In Sec.2, both FDTD algorithm and prototype (discrete human head and phone) models are eqplained. Mobile cellular phone transmitter, radiation boundary treatment and SAR evaluation processes are presented in this section. Then, in Sec.3, various SAR distribution calculations are performed and the results are evaluated in terms of safety limits given in [2]. Finally, the conclusions are outlined in Sec.4.

2. FDTD and SAR Evaluation Process

2.1. FDTD Method

As indicated by its name, FDTD method solves Maxwell's equations directly in time domain. Assuming a piecewise uniform, homogeneous, isotropic and lossy media, source-free Maxwell's curl equations

$$\mu_0 \frac{\partial \vec{H}}{\partial t} = -\nabla \times \vec{E} \tag{1}$$

$$\varepsilon \frac{\partial \vec{E}}{\partial t} = \nabla \times \vec{H} - \sigma \vec{E} \tag{2}$$

are discretized both in space and time with (i, j, k) and n representing the discrete space and time nodes,

$$E_x(x, y, z, t) = E_x^n(i, j, k); x = i \times \Delta x, y = j \times \Delta y, z = k \times \Delta z, t = n \times \Delta t \tag{3}$$

respectively. All six components of electromagnetic fields are located at specific points of unit cells as suggested by Yee [14], where $\vec{E}$ and $\vec{H}$ are interleaved in both space and time. This FDTD arrangement is shown in Figure 1. Here, electric field components E_x, E_y, E_z are located on the three edges and magnetic field components H_x, H_y and H_z are located in the middle of the three surfaces and are assumed contant. In addition to one-half spatial-cell displacement between $\vec{E}$ and $\vec{H}$, there is also one-half time-cell displacement.

Applying the discretization and rearranging the equations suitable to iterative calculations yield,

$$\begin{aligned} H_x^{\vec{n}}(i,j,k) = H_x^{\vec{n}-1}(i,j,k) &- \frac{\Delta t}{\mu_0 \Delta z}[E_y^n(i,j,k) - E_y^n(i,j,k-1)] \\ &- \frac{\Delta t}{\mu_0 \Delta y}[E_z^n(i,j,k) - E_z^n(i,j-1,k)] \end{aligned} \tag{4}$$

$$\begin{aligned} H_y^{\vec{n}}(i,j,k) = H_y^{\vec{n}-1}(i,j,k) &- \frac{\Delta t}{\mu_0 \Delta x}[E_z^n(i,j,k) - E_z^n(i-1,j,k)] \\ &- \frac{\Delta t}{\mu_0 \Delta z}[E_x^n(i,j,k) - E_x^n(i,j,k-1)] \end{aligned} \tag{5}$$

$$\begin{aligned} H_z^{\vec{n}}(i,j,k) = H_y^{\vec{n}-1}(i,j,k) &- \frac{\Delta t}{\mu_0 \Delta y}[E_x^n(i,j,k) - E_x^n(i,j-1,k)] \\ &- \frac{\Delta t}{\mu_0 \Delta x}[E_y^n(i,j,k) - E_y^n(i-1,j,k)] \end{aligned} \tag{6}$$

$$E_x^n(i,j,k) = \frac{2\varepsilon - \sigma \Delta t}{2\varepsilon + \sigma \Delta t} E_x^{n-1}(i,j,k) - \frac{2\Delta t}{(2\varepsilon - \sigma \Delta t)\Delta z}[H_y^n(i,j,k) - H_y^n(i,j,k-1)]$$

$$+ \frac{2\Delta t}{(2\varepsilon - \sigma\Delta t)\Delta y}[H_z^n(i,j,k) - H_z^n(i,j-1,k)] \tag{7}$$

$$E_y^n(i,j,k) = \frac{2\varepsilon - \sigma\Delta t}{2\varepsilon + \sigma\Delta t}E_y^{n-1}(i,j,k) - \frac{2\Delta t}{(2\varepsilon - \sigma\Delta t)\Delta x}[H_z^n(i,j,k) - H_z^n(i-1,j,k)]$$
$$+ \frac{2\Delta t}{(2\varepsilon - \sigma\Delta t)\Delta z}[H_x^n(i,j,k) - H_x^n(i,j,k-1)] \tag{8}$$

$$E_z^n(i,j,k) = \frac{2\varepsilon - \sigma\Delta t}{2\varepsilon + \sigma\Delta t}E_z^{n-1}(i,j,k) - \frac{2\Delta t}{(2\varepsilon - \sigma\Delta t)\Delta y}[H_x^n(i,j,k) - H_x^n(i,j-1,k)]$$
$$+ \frac{2\Delta t}{(2\varepsilon - \sigma\Delta t)\Delta x}[H_y^n(i,j,k) - H_y^n(i-1,j,k)] \tag{9}$$

where $\tilde{n} = n + 1/2$. In eq.s (4)-(9), it is assumed that no magnetic materials are present so that each cell is characterized by constant medium parameters μ_0, ε and σ given for the reference point of the cell.

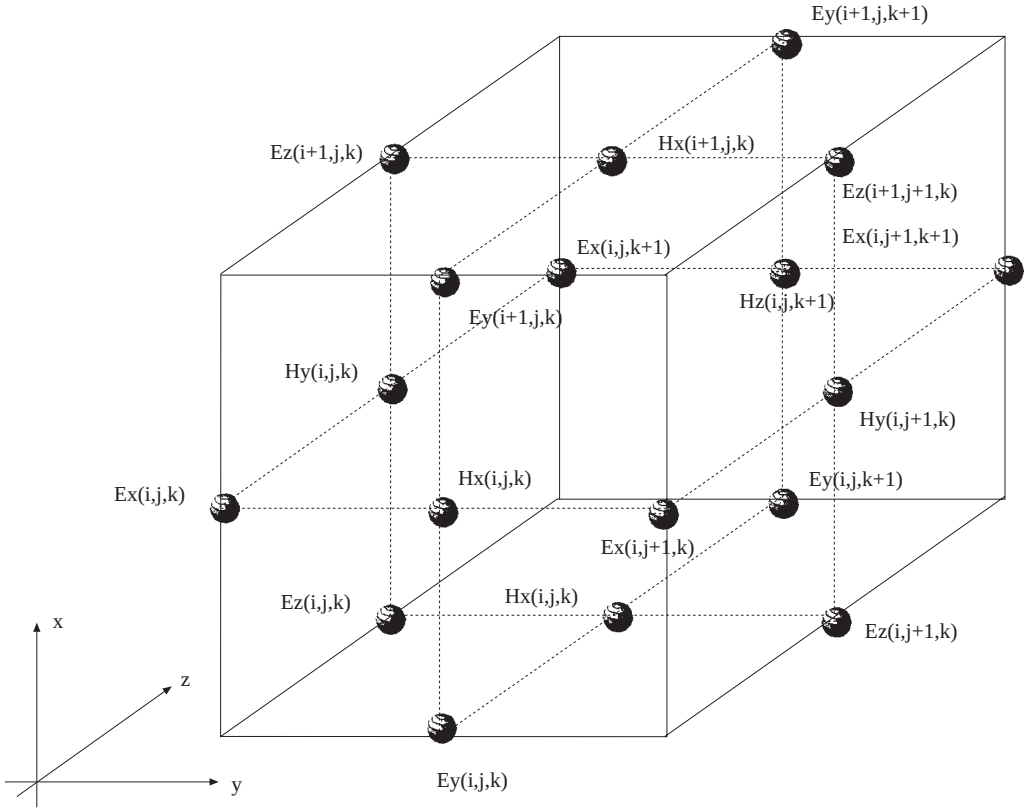

Figure 1. FDTD unit cell suggested by Yee and locations of EM field components.

FDTD method is mainly based on calculation of eq.s (4)-(9), with suitable excitation representation and with satisfaction of the necessary boundary conditions at $t_n = n \times \Delta t$ time instants. The most important points in FDTD calculations are the stability and numerical dispersion [18]. Since, FDTD algorithm is based on iterative calculations of six field components, a certain relation between spatial and time intervals

$$\Delta t \leq \frac{1}{c\sqrt{(\frac{1}{\Delta x})^2 + (\frac{1}{\Delta y})^2 + \left(\frac{1}{\Delta z}\right)^2}}; c = 3 \times 10^8 m/s \;\; free - space EM wave velocity \tag{10}$$

needs to be satisfied for stability (named as Courant criteria) [16]. Similarly, the spatial discretization must be done to allow to trace the highest frequency (minimum wavelength) component in the desired frequency band (numerical dispersion).

2.2. Configuration in FDTD

The basic configuration within FDTD volume in cartesian coordinates system is shown in Figure 2 where discretized human head and hand-held cullular mobile phone are placed. The region of interest extends from the coordinate origin (0,0,0) to X_{max} , Y_{max} , Z_{max}). FDTD computation volume is a rectangular box made up with $Nx \times Ny \times Nz$ unit cells. where $Nx = X_{max}/\Delta x, Ny = Y_{max}/\Delta Y Nz = Z_{max}/\Delta z$. FDTD volume is bounded by six boundary surfaces, where special treatment is necessary as explained in Sec.2.3. Typical dimensions of the FDTD volume is taken as $Nx = 50$, $Ny = 50$, $Nz = 50$ with a total of 125.000 cubic cells. The cell sizes are chosen to be $\Delta x = \Delta y = \Delta z = 0.65cm$, which means that a cubic volume of $32.5cm \times 32.5cm \times 32.5cm$ is allocated for FDTD calculations where human head and hand-held cellular phone are located.

A realistic and accurate near field box model is used to simulate the cellular mobile phone. This model consists of an infinitely thin quarter-wavelength wire antenna (monopole) placed on a perfectly conducting rectangular box. As shown in Figure 2, hand-held cellular phone is represented with the box model used by [10] and [15]. The dimensions of hand-held cellular phone is 3.25cm in x, 6.5cm in y and $13cm$ in z. Total of $5 \times 10 \times 20$ cubic cells are reserved for hand-held cellular phone and is located 3 cells (1.95 cm) away from the human head model at the level of right ear. A quarter-wavelength (infinitely thin) monopole (13 cells in 900 MHz and 6 cells in 1.8 GHz) is mounted on top of the box model (paralel to z axis). Between wire antenna and the box, one unit-cell gap is available for excitation of the antenna. Along the wire antenna longitudinal component of electric field is set to zero to simulate perfectly electric conductor (PEC). The case of the box is modeled with a plastic cover (with ε_r=2.2 as in [8]) and the internal circuitry with a good conductor (equal to the copper value, $\sigma = 5.8 \times 10^7 S/m$). Total of 1000 cubic cells are used for the box model given in Figure 2.

A three dimensional (3D) EM model of a human head is derived from an NMR image. The gray levels in NMR image are traced with a semi-automatic algorithm to separate brain, muscle, fat, bone and other tissu types [8]. In FDTD volume, human head is represented with 24 vertical slices (in yz planes) located along the x axis, with nose pointing positive y direction (see Figure 2). The dimensions of the discretized human head model in cubic-cells are 24 by 33 by 31 in x, y, and z directions, respectively. This corresponds to $15.6cm \times 21.5cm \times 20cm$ cubic volume. The human head model is located 10 cells away from $x = 0$, $y = 0$ and $z = 0$ planes. The tissue types, number of occupied cubic cells and their electrical properties at two operating frequencies are listed in Table 1 [8]. As listed in Table 1, seven different tissues are used in discretized model of the human head. It should be noted that, as much as 120 tissue types can be obtained and used while discretization of the NMR image [10]. Since the SAR distribution is calculated over a certain amount of tissue, highly distributed small scale tissues are not taken into account in this model. Also, average brain tissue is used instead of brain with grey and white matters [8]. The discretized form of the human head model is shown in Figure 3 at horizontal and vertical slices, respectively, where the slice numbers are mentioned. Although some are indistinguishable, all the tissues in the head are represented with defferent gray tones. Total of 24552 cubic cells are used for the human head model. Nearly half of these cubic cells are occupied by the tissues (12192) and the rest (12360) are modeled as free-space. As a result, nearly 10 percent of the FDTD volume is occupied by the discrete human head model and 1 percent is occupied by the box model for hand-held cellular phone.

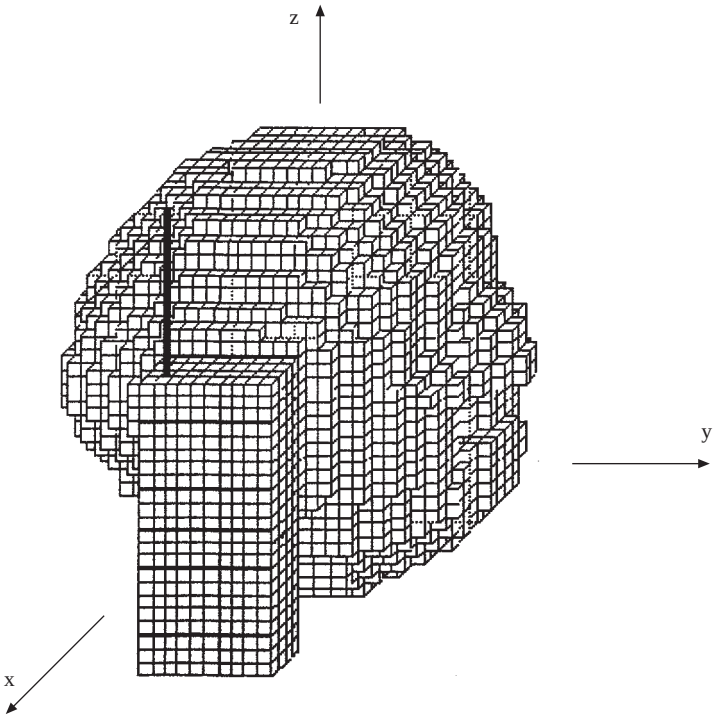

Figure 2. Discrete human head and hand-held cellular phone models.

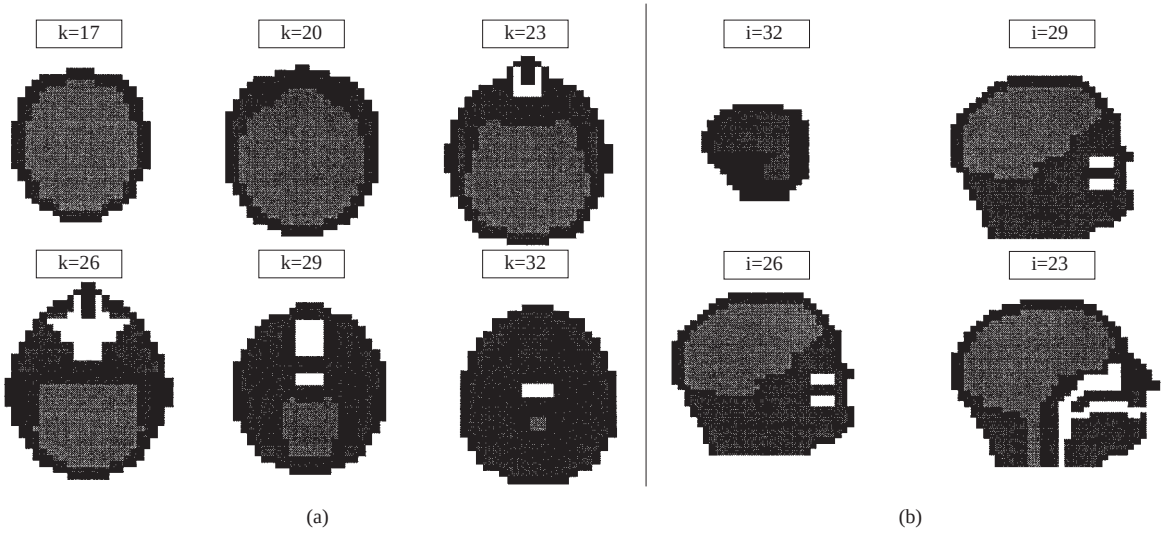

Figure 3. Horizontal (k=17, 20, 23, 26, 29, 32) and vertical (i=32, 29, 26, 23) slices of human head model showing different tissues.

2.3. Source and Boundary Implementation in FDTD

Since the computational space of FDTD solution must be truncated because of finite limitation of computer storage capacity, the boundary surfaces need special treatment to simulate open regions. There are quite a few Radiation Boundary Conditions (RBC) used for different type of EM problems. First and second order dispersive boundary conditions (DBC) [22, 23] and modified DBC [24] are especially well-suited to planar

microstrip structures. On the other hand, in antenna simulation and radar cross-section (RCS) analysis first and second order Mur [25] boundary conditions are used. In this study, first order Mur simulations are used at the edges and corners and second order Mur is used everywhere else on the boundary surfaces.

In Yee arrangement [14], there are two tangential electric and one normal magnetic field components at each boundary plane. For example, at $x = Xmax$ plane, the tangential electric field components are E_z and E_y and the normal magnetic field component is H_x. Since, H_x at this boundary is calculated in terms of E_z and E_y (see eq.(4)), only tangential electric field components at the boundary planes are used to simulate RBCs.

For the first order Mur [25] RBC along x direction

$$\left[\frac{\partial}{\partial x} - \frac{1}{c}\frac{\partial}{\partial t}\right] E_y = 0 \quad \text{and} \quad \left[\frac{\partial}{\partial x} - \frac{1}{c}\frac{\partial}{\partial t}\right] E_z = 0 \tag{11}$$

should be satisfield at both $x = 0$ and $x = Xmax$ planes. FDTD discretized form of eq(11) at $x = 0$ boundary plane will then be (for E_z component)

$$E_z^{n+1}(1,j,k) = E_z^n(2,j,k) + \frac{c\Delta t - \Delta x}{c\Delta t + \Delta x}[E_z^{n+1}(2,j,k) - E_z^n(1,j,k)]. \tag{12}$$

This condition allows to absorb the plane waves propagating with velocity c towards $x = 0$. However, waves with spherical wavefronts need higher order conditions at these boundary planes. The second order Mur [25] for of the same boundary simulation is given as

$$\begin{aligned} E_z^{n+1}(1,j,k) \;=\; & -E_z^{n-1}(2,j,k) + \left(\frac{c\Delta t - \Delta x}{c\Delta t + \Delta x}\right)[E_z^{n+1}(1,j,k) + E_z^{n-1}(1,j,k+)] \\ & + \left(\frac{2\Delta x}{c\Delta t + \Delta x}\right)[E_z^n(2,j,k) + E_z^n(1,j,k+)] \\ & + \left(\frac{(c\Delta t)^2}{2\Delta x(c\Delta t + \Delta x)}\right)[E_z^n(1,j+1,k) - 2E_z^n(1,j,k) \\ & + E_z^n(1,j-1,k) + E_z^n(2,j+1,k) - 2E_z^n(2,j,k) + E_z^n(2,j-1,k) \\ & + E_z^n(1,j,k+1) - 2E_z^n(1,j,k) + E_z^n(1,j,k-1) + E_z^n(1,j,k) \\ & - 2E_z^n(2,j,k) + E_z^n(2,j,k-1)]. \end{aligned} \tag{13}$$

Recently, a new and effective absorbing boundary simulation, perfectly matched layer (PML), is introduced for the cases, where high accuracy is essential [26]. Although it increases the simulation time and storage requirements, PML and its other implementations [27] give quite high performances, especially for antenna arrays and RCS calculations [28,29].

Typical excitation of wire antenna geometries in FDTD calculations is performed using a gap voltage in one cell left for the feed point [15]. In this study, the z-directed quarter wave-length monopole antenna located one cell above the box model is excited at the source cell with a voltage source V_s

$$E_z^n(i_s,j_s,k_s) = E_z^n(i_s,j_s,k_s) + \frac{V_s(n\Delta t)}{\Delta z} \tag{14}$$

where (i_s, j_s, k_s) represents the labels of the source cell, the gap between the wire antenna and the box model. For this voltage source model, current flowing through the wire antenna is calculated from Ampere's law

$$I_s(\tilde{n}) = [H_x^{\tilde{n}}(i,j,k) - H_x^{\tilde{n}}(i,j+1,k)]\Delta x + [H_y^{\tilde{n}}(i,j,k) - H_y^{\tilde{n}}(i+1,j,k)]\Delta y \tag{15}$$

and the time ofset of $\Delta t/2$ between source voltage and current is generally neglected since it is assumed to be small. The time step Δt is taken as 12.5ps for 900MHz calculations. Hence one period corresponds to $89\,\Delta t$ for sinuzoidal voltage. The simulation time is fixed to 1500 time steps (nearly 17 periods), which is larger than 3-5 periods necessary to reach the steady state regime.

2.4. Power Calculations and SAR Evaluation

With the source simulation described above, attention should be paid to power radiated from the hand-held cellular phone, radiation impedance of the antenna and total power absorbed in the human head. Power radiated from the antenna can be calculated in two different ways. First way is based on the calculation of free-space radiation impedance (Z_{R_0}). Assuming the source has an impedance equal to complex conjugate of the free-space radiation impedance $(Z_s = Z_{R_0})$, radiated power (600mW for 900MHz) is obtained directly from [10]

$$V_s(i_s, j_s, k_s) = \sqrt{8 \times 0.6 \times R_{R0}} \tag{16}$$

where $R_{R0} = Re\{Z_{R0}\}$. The radiation impedance Z_{R0} is obtained from the maximum amplitude of the current (calculated from eq.(15)) and the phase difference between the current and impressed voltage.

The second way to compute the total radiated power is to integrate Poynting vector over a closed surface around the hand-held cellular phone antenna (excluding the human head model);

$$P_{rad} = \int\int_S (\vec{E} \times \vec{E})\vec{u}_n dS \tag{17}$$

where $\vec{u}_n$ is the unit vector perpendicular to the surface S and pointing outward of the volume. In this study, Poynting vector is calculated at each time step and integrated over a closed surface enclosing a rectangular volume which contains the discrete models. First, the human head model is removed from FDTD volume and antenna power is calculated after the steady state regime has been reached. Then, discrete human head model is placed within FDTD volume and the same closed surface integration of Polynting vector is carried out to find out the radiated power. Since the head model contains lossy dielectric tissues, the difference between these two power values is the absorbed power within the tissues.

For SAR evaluations, total power absorbed in human head should be calculated during FDTD simulation. The absorbed power P_{abs} is related to the conductivity (σ) of different tissues in head and determined by integrating the absorbed power density over the volume V of the human head model;

$$P_{abs} = \int\int\int_V \frac{\sigma(\vec{r})}{2} |\vec{E}\vec{r}|^2 dV \tag{18}$$

where $\vec{r}$ represents coordinate of the cell under evaluation. The conductivity $\sigma(\vec{r})$ is in Siemens per meter, and electric field strength $\vec{E}(\vec{r})$ is in volts per meter. Finally, the local SAR is computed from

$$SAR = \frac{\sigma}{2\rho}|\vec{E}|^2 \quad [W/kg] \tag{19}$$

with $\rho, [kg/m^3]$ representing density of the tissue.

3. Numerical Implementations

As mentioned in Sec.2.4., eq.s(17)-(19) are used for the radiated power, absorbed power and SAR computations, respectively. The first numerical tests are done to evaluate the antenna output, radiated and absorbed powers. To find out the antenna output power, first human head model is removed from FDTD volume and antenna is excited as given in eq.(14). FDTD computational space is a cubic volume made up by hundreds of thousands cubic Yee [14] cells (see Figure 1). Second inner cubic volume (5-10 cells away from boundaries) is chosen for the power calculations. Poynting vector is integrated for every cell on six square surfaces closing this volume. Since FDTD volume is free-space and contains only the hand-held cellular phone, this integration yields the antenna output power. In Figure 4 the time variation of the antenna power obtained by closed surface integration of Poynting vector is plotted. Here, positive values correspond to net outward power flow. Solid and dashed lines in Figure 4 correspond to instantaneous and average powers, respectively. At 900MHz operating frequency, one period corresponds approximately to 1.1 ns ($89\Delta t$) and time variation is given for 15ns. The transient effects within 4-5 periods, and steady-state settlement of the power thereafter is clearly seen in Figure 4. The gap voltage in eq.(14) is chosen as to give an average transmitted power of 600mW (see Figure 4).

After calculating the transmit power of hand-held cellular phone, the human head model is located within FDTD volume as explained in Sec.2.2. Similar closed surface integration of Poynting vector is carried out for this case. Both instantaneous and average powers are again plotted in Figure 5. As seen from Figure 5, the average power leaving the volume is calculated to be 464mW. This is the radiated power and the difference between transmitted and radiated powers (600-464=136mW) must be the power absorbed in human head. The absorbed power in human head is also calculated from the volume integral given in eq.(18). All the time variations of the average powers are plotted in Figure 6. The absorbed power in human head, calculated from the volume integral in (18) by using conductivity values of the different tissues, is obtained to be 139mW. The relative difference between two values of absorbed power is about 2%. The electric field components in Yee cell are located at different edges as explained in Sec.2.1. Averaging these field components at the same point in each cell and then evaluating the volume integral yields better agreement in absorbed power. Better than 1% agreement is obtained in power calculations for both GSM and DECT systems. The results in Figure 6 show that after the transient time period (3-5 periods) an excellent agreement in power conservation is obtained in FDTD calculations. The instantaneous powers are also plotted with respect to time in Figure 7. Here, solid and dashed lines correspond to antenna power and total of absorbed plus radiated powers, respectively. Before doing the SAR calculations given below, the degree of the numerical errors caused by discretization (i.e., cell sizes) is also tested. A spherical, homogeneous test tissue is located inside the FDTD volume and power calculations are done with different cell sizes. The parameters are chosen in such a way that discretization errors are negligible (i.e., less than two percent).

For GSM system (i.e., at 900MHz), the peak SAR distributions are calculated via eq.(19). Maximum peak SAR, averaged over one period, is obtained as 1.2W/kg which has a normalized value of 1.93 or 2.85dB. This value is obtained in *muscle* (numbered as 3) at cell (32,27,26). In Figure 8, peak SAR distributions are given at six horizontal slices mentioned in Figure 3a with the dynamic range of 40dB. Similarly, SAR distributions at four vertical slices mentioned in Figure 3b are plotted in Figure 9. The peak SAR values, averaged in one period, are 2.85dB, -0.04dB, -4.36dB and -9.17dB at these vertical slices, showing the range dependence of peak SAR. In all figures, high SAR values are in black and are obtained near the antenna feed point.

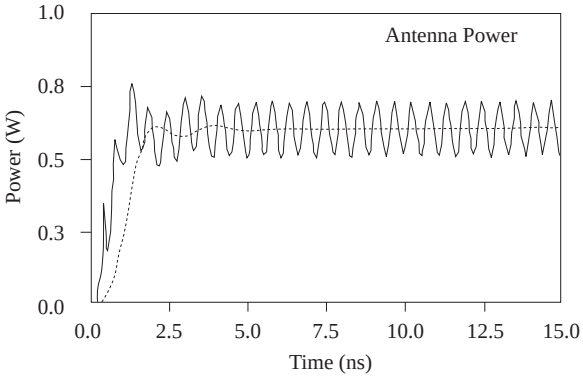

Figure 4. Time variation of the antenna power calculated with a closed surface integration of Polynting vector (solid: instantaneous power, dashed: average power, human head model removed)

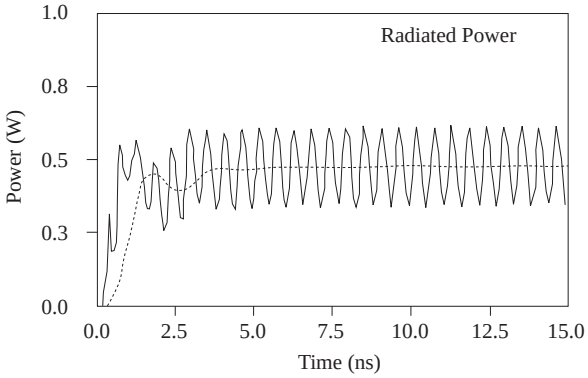

Figure 5. Time variation of the radiated power calculated with a closed surface integration of Polynting vector (solid: instantaneous power, dashed: average power, with human head model)

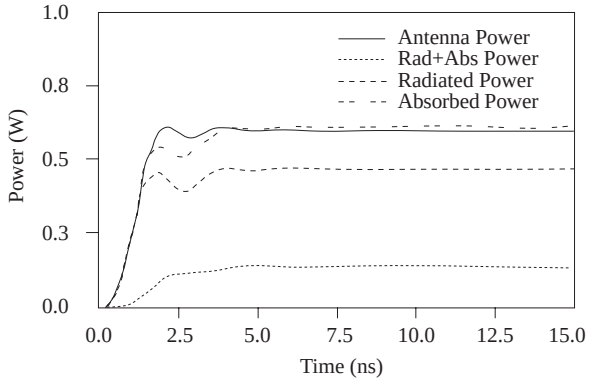

Figure 6. Time variations of average power calculated during FDTD simulation with both two dimensional closed surface and three dimensional volume integrations given in eq.s(17)-(19).

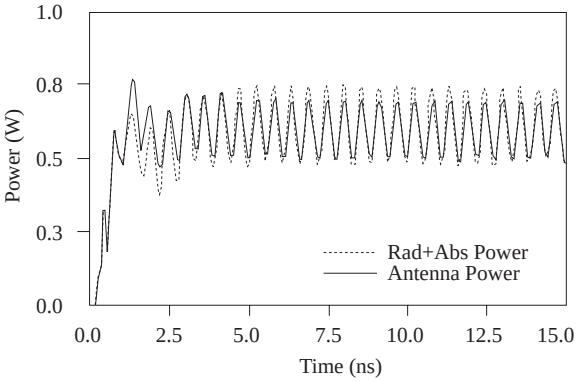

Figure 7. Time variations of instantaneous power calculated during FDTD simulation with both two dimensional closed surface and three dimensional volume integrations given in eq.s(17)-19).

The same computations are carried out for European DECT system (i.e., at 1800 MHz operating frequency) by using quarter-wavelenth antenna mounted on top of the box model and the transmitted power of 250mW. In Figure 10, time variations of both antenna power and radiated+absorbed powers are plotted. Excellent agreement between the results are clearly seen from the figure. Finally, peak SAR distributions for DECT system are given in Figure 11 and 12, at the same horizontal and vertical slices used for GSM (i.e., 900 MHz) calculations, respectively. Also, the power scales in both calculations are same (i.e., normalized to antenna power). Compared to Figure 8, the peak SAR distributions are low in DECT system throughout all six horizontal slices shown in Figure 11. For the vertical slices, the maximum peak SAR value for each system is obtained at the same vertical plane (slice (a)). For DECT system, maximum peak SAR averaged over one period, is obtained as 0.75W/kg which has a normalized value of 3.08 or 4.89dB. This value is again detected in the same tissue, numbered as 3 (corresponds to *muscle*) but at slightly different cell (32, 24, 28), which is nearer to antenna feed plane than the one obtained for GSM system. The peak SAR values at 1.8GHz, averaged over one period, are 4.89dB, -5.34dB, -11.28dB and -15.04dB at these vertical slices. This

shows that the decrease in absorbed power with respect to distance is steeper in DECT compared to GSM system.

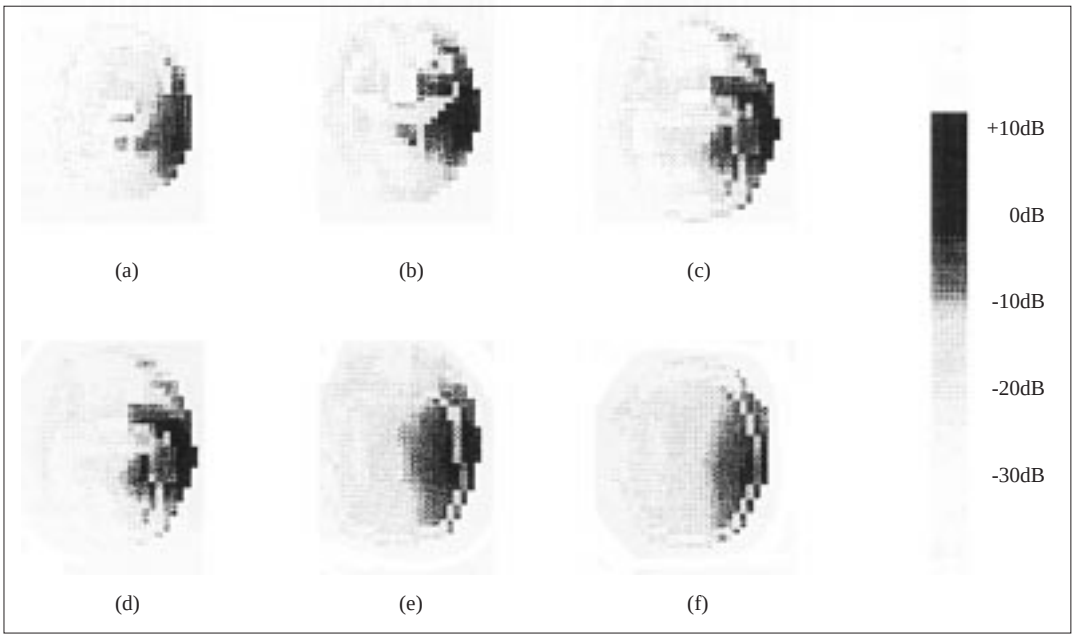

Figure 8. Peak SAR distributions at six different horizontal slices (k=17, 20, 23, 26, 29, 32) given in Figure 3a. Maximum value is obtained in (d) at (32,27,26)

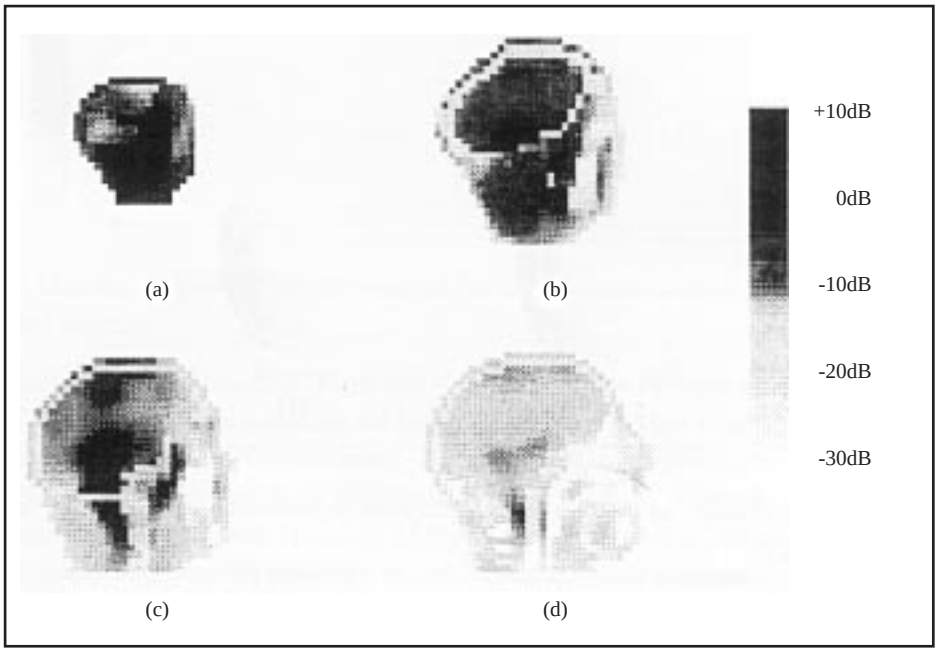

Figure 9. Peak SAR distributions at four different vertical slices given in Figure 3b (i=32, 29, 26, 23). Maximum value is obtained in (a) at (32.37.26)

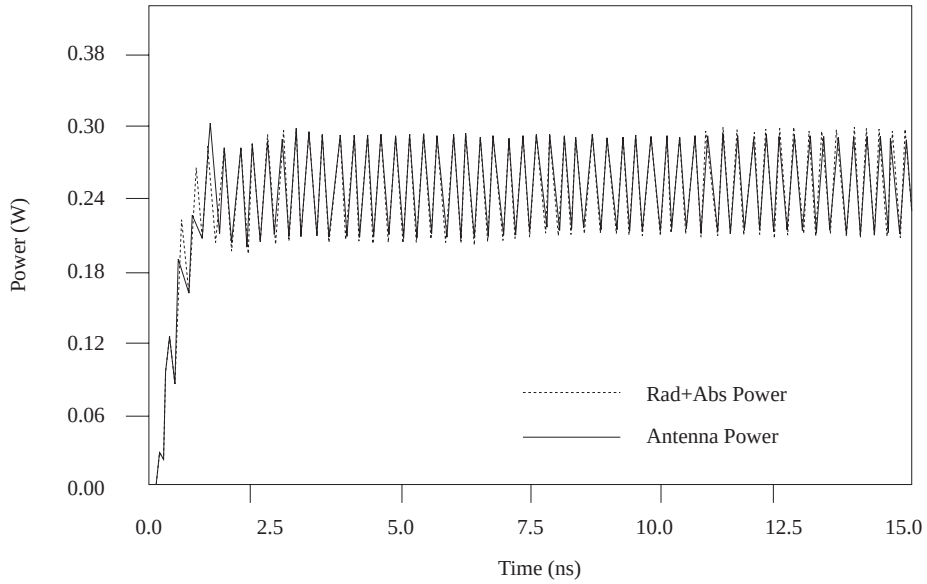

Figure 10. Time variations of instantaneous values of both antenna and radiated+absorbed powers for DECT system (f=1.8 GHz and antenna output power 250mW)

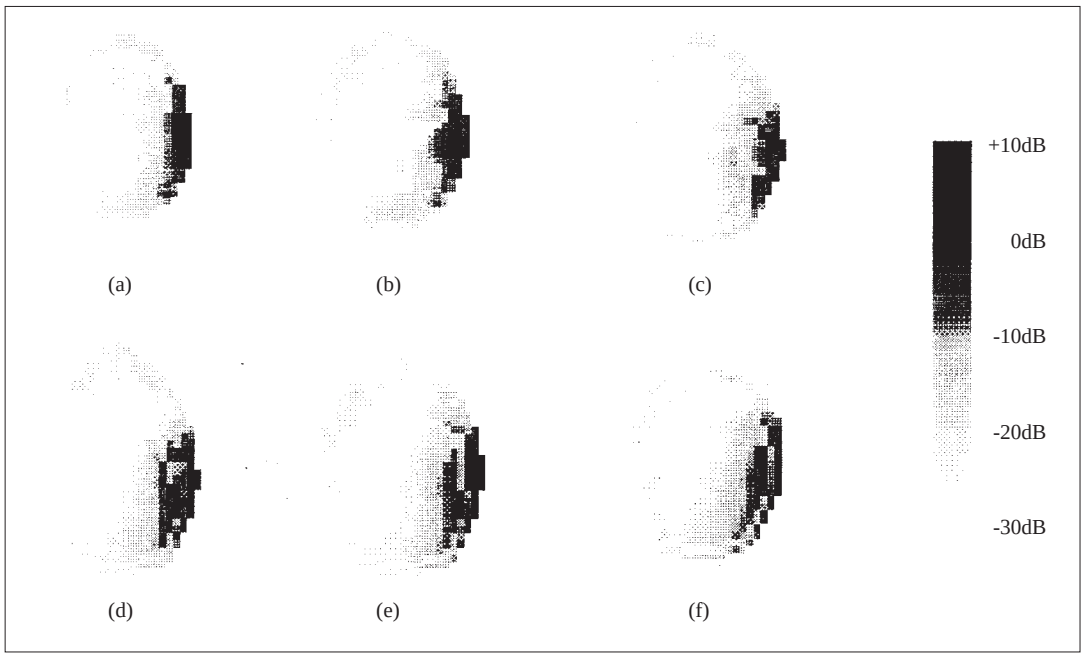

Figure 11. Peak SAR distributions for DECT system at the same six horizontal slices given in Figure 8. Maximum value is obtained at (32.24.28)

4. Conclusions

In this study, the effects of hand-held cellular phones to isolated human head is studied with FDTD method. The SAR distribution in a human head exposed to EM field emitted from a hand-held cellular phone is

calculated for both GSM (i.e, at 900 MHz) and DECT (i.e, at 1.8 GHz) systems. Particular attention has been given to accurate power calculations. In order to give dependable compuational results input and radiated powers must be accurately calcuated. Here, the surface integration of the Poynting vector with and without human head model and the volume integration of the absorbed power are calculated separately and the results are shown to agree very well. Accurate SAR calculations are done within the limits of the used discrete models and EM parameters and agreement with the results in the literature is obtained. The peak SAR values, over any 1 g of tissue for phones radiating 600mW (for GSM) and 250mW (for DECT) of power in free-space are obtained and are shown to be below the ANSI safety limits. It should be mentioned that, the safety limits themselves are uncertain because of the complex EM behaviors of human tissues. This may be directly observed in the differences of the limits of the European and American safety organisations. These numerical simulations and the laboratuary measurements based on human prototypes should accompany long term medical investigations in order to talk about the safety limits of these electronic devices.

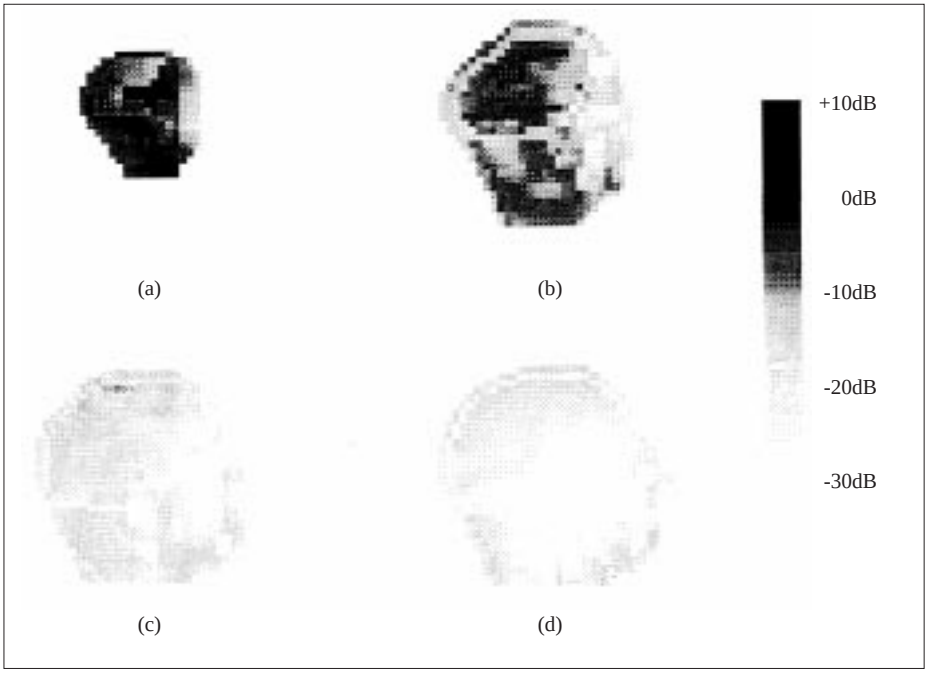

Figure 12. Peak SAR distributions for DECT system at the same vertical slices given in Figure 9. Maximum value is obtained in a) at (32.37.26).

The comparisons of GSM and DECT systems show the relation between antenna and absorbed powers in human tissues. As given in Table 1, tissues are lossy dielectrics and their conductivity values increase with frequency. As the operating frequency increases, the peak SAR value increases as expected from eq.(19), but total absorbed power in human head decreases, because of the decrease in penetration of EM fields through tissues. Optimisation between the peak SAR and total absorbed power should be made in choosing the operating frequency and antenna power for mobile communication systems.

FDTD is a powerful technique to calculate EM effects in environments where human tissues are present beside electronic devices. The presented algorithm may be used directly to test various antenna types as well as antenna orientations. Also, the effects of the human head to the antenna radiation pattern and efficiency may be calculated with the same FDTD algorithm, by applying time-domain near-to-far field followed by discrete Fourier transforms [1] [19].

Table 1. Tissue types, number of model cubes, their densities and electrical propeties used in FDTD calculations.

			Frequency	900MHz		1.8GHz	
	Tissue	Cells	$\rho[kg/m^3]$	ε_r	$\sigma[S/m]$	ε_r	$\sigma[S/m]$
0	Air	12360	-	1.00	0.00	1.00	0.00
1	PEC	-	-	-	$\propto$	-	$\propto$
2	Bone	2188	1850	8.00	0.11	8.00	0.16
3	Skin/fat	2318	1100	34.50	0.60	32.99	0.52
4	Muscle	3490	1040	58.50	1.21	55.00	1.90
5	Brain	4066	1030	55.00	1.23	53.00	1.70
6	Humour	16	1010	73.00	1.97	75.00	2.40
7	Lens	8	1050	44.50	0.80	41.00	1.29
8	Cornea	106	1040	52.00	1.85	50.00	2.32

Numerical modeling of human head-cellular phone is a very important problem. The importance of the problem has just been re-evaluated in a special session of an IEEE AP-S conference [30], where the most recent studies of the well-known groups were presented and discussed. In that conference, the points listed below were especially mentioned by all of the researches:

- There is a great demand to build a canonical head, hand, neck and phone models, where the results of all the algorithms may then be compared on the same platform.
- Care should be given when using box or sphere or other simple models for the worst case SAR calculations, because of extreme difficulty in worst case definition.
- Since it does not account for the tissue dosimetry, the FDTD based SAR calculations should be evaluated in connection with the medical research society.
- Accuracy of these numerical simulations strongly depend on the reliability of electrical parameters of the tissues. Therefore, parallel studies should be continued with groups who conduct measurement researches.
- Finally, long term meaurements, simulations and statistical evaluations should be done before making any declerations related to public health and safety.

References

[1] L. Sevgi and S. Paker, Fdtd based rcs calculations and antenna simulations. *AEU, International J. of electronics and Communication,* Vol.52, NO:2, pp.65-75. March 1998.

[2] ANSI/IEEE C95.1-1992. *American National Standard-safety Levels with Respect to Exposure to Radio Frequency Electromagnetic Fields, 3kHz to 300GHz.* New York, IEEE.

[3] Int. Non-lonizing Rad. Committe of the Int. Rad. Protec. Assoc. Guidelines on limits of exposure to radio frequency em fields in the frequency range from 100kHz to 300GHz. *Health Physics,* V 54-1, pp. 115-123, 1988.

[4] Q. Balzano O. Garay, F. R. Steel. Heating of biological tissue in the induction field of VHF portable radio transmitters. *IEEE Trans. Veh. Technol.,* VT-27, pp. 51-56, 1978.

[5] Q. Balzano O. Garay, F. R. Steel. Energy deposition in simulated human operators of 800MHz portable transmitters. *IEEE Trans. Veh. Technol.,* VT-27, pp.174-181, 1978.

[6] K. H. Joyner V. Anderson. Specific absorbtion rate levels measured in a phantom head exposed to radio frequency transmissions from analog hand-held mobile phones. *Bioelectromagn.,* V 16, pp. 60-69, 1995.

[7] P. J. Dimbylow. Fdtd calculations of the sar for a dipole closely coupled to the head at 900MHz and 1.9GHz. *Phys. Med. Biol.,* V 38, pp.361-368, 1993.

[8] Y. Rahmat-Samii M. A. Jensen. Performance analysis of antennas for hend-held transsreceivers using FDTD. *IEEE Trans. Antennas and Propagat.,* V 42, No 8, pp.1106-1112, 1994.

[9] O.P. Gandhi G. Lazzi, C.M. Furse. Electromagnetic absorbtion in the human head and neck for mobile telephones at 835 and 1900 MHz. *IEEE Trans. Microwave Theory Tech.,* MTT-44, No 10, pp.1884-1897, 1996.

[10] L. Martens J. De Moerloose, De Zutter. Calculation of the electromagnetic fields induced in the head of an operator of a cordless phone. *Radio Science,* Vol 30, No 1. pp. 283-290, 1995.

[11] S. Watanabe M. Taki, T. Nojima O. Fujiwara. Characteristics of the sar distributions in a head exposed to electromagnetic fields radiated by a hand-held portable radio. *IEEE Trans. Microwave Theory Tech.,* MTT-44, No 10, pp.1874-1883, 1996.

[12] M. A. Stuchly, M. Okoniewski. A study of the handset antenna and human body interaction. *IEEE Trans. microwave Theory Techl,* MTT-44, No 10, pp.1855-1864, 1996.

[13] P. J. Dimbylow and S. M. Mann. Sar calculations in an anatomically based realistic model of the head for mobile communication transreceivers at 900MHz and 1.8GHz. *Physics in Medicine Biology,* Vol-39, pp.1537-1553, 1994.

[14] K. S. Yee. Numerical solution of initial boundary value problems involving maxwell's equations in isotropic media. *IEEE Trans. antennas and Propagat.,* AP-14, pp.302-307, 1966.

[15] R. J. Luebbers, K. S. Kunz. *The Finite-difference Time-Domain Method for electromagnetics.* CRC Press, Boca Raton, FL, 1993.

[16] A. Taflove. *Computational Electrodynamics: The Finite-Difference Time-Domain Method.* Artech House, Norwood, MA, 1995.

[17] D. M. Sheen, S. M. Ali, M. D. Abouzahra, J. A. Kong. Application of the finte-difference time-domain method to the analysis of microstrip discontinuites. *IEEE Trans. Microwave Theory Tech.,* MTT-38, No 7, pp.849-857, 1990.

[18] K. K. Mei, X. Zhang. Time-domain finite-difference approach for the calculation of the frequency-dependent characteristics of microstrip discontinuities. IEEE Trans. Microwave Theory Tech., MTT-36, pp. 1775-1787, 1988.

[19] F. Akleman and L. Sevgi. Fdtd analysis of human head-mobile phone interaction in terms of specific absorbtion rate (sar) calculations and antenna design. *IEEE-APS, Proc. of Conference on antennas and Propogation for Wireless Communications,* pp. 85-88, November 2-4, Waltham, MA, USA,1998.

[20] F. Akleman and L. Sevgi. Radar cross section and antenna modeling with fdtd method. Proc. of *JINA'98, Int. Symp. on Antennas,* November 17-19, France, 1998.

[21] M. Orhan Ozyalcın and L. Sevgi. Comparisons of fdtd and tlm methods in shielding effect analysis. *Proc. of IEEE CEFC'98 the eight Biennial IEEE Conference on Electromagnetic field Computattion,* June 1-3, Tuscon, Arizona, USA, 1998.

[22] Z. Bi K. Wu, C. Wu J. Litva. A dispersive boundary condition for microstrip component analysis using the fd-td method. *IEEE Trans. Microwave Theory Tech.,* MTT-40, pp.774-777, 1992.

[23] C. Wu K. Wu Z. Bi, J. Litva. Accurate characterization of planar printed antennas using finite-difference time-domain method. *IEEE Trans. antennas and Propagat.,* Ap-40, No 5, pp. 526-533, 1992.

[24] R. Mitra, V. Betz. Comparison and evaluation of boundary conditions for the absorbtion of guided waves in an fdtd simulation. *IEEE Microwave Guided Lett.,* Vol 2, pp.499-501, 1992.

[25] G. Mur. Absorbing boundary conditions for the finite-difference approximation of the time-domain electromagnetic field equations. *IEEE Trans. Electromag. Compat.,* EMC-23, pp.377-382, Nov. 1981.

[26] J. P. Berenger. A perfectly matched layer for the absorbtion of electromagnetic waves *J. Compuational Physics,* Vol.114, pp.185-200, 1994.

[27] F. Akleman and L. Sevgi. A novel implementation of berenger's pml for fdtd applications. *IEEE Microwave Guided Lett.,* Vol.8, No 10, pp.324-327, Oct. 1998.

[28] L. Sevgi, F. Akleman. Radar cross-section (rcs) modeling and stealth target design. Int. J. of numerical modeling, (submitted), Aug. 1998.

[29] L. Sevgi, F. Akleman. Radar cross section analysis of canonical structures. *Canadian J. of Electrical Computer Engineering,* (submitted), Oct. 1998.

[30] *IEEE-APS, Conference on Antennas and Propagation for Wireless Communications,* Waltham, MA, USA, Nov.2-4, 1998.